Electron Localization in Non-Compact Covalent Bonds Captured by the r^{2}SCAN+V Approach

Yubo Zhang[1,*], Da Ke[1], Rohan Maniar[3], Timo Lebeda[3], Peihong Zhang[2,*], Jianwei Sun[3,*], John P. Perdew[3,*]

[1]*Minjiang Collaborative Center for Theoretical Physics, College of Physics and Electronic Information Engineering, Minjiang University, Fuzhou, China*

[2]*University at Buffalo, State University of New York, Buffalo, New York 14260, USA*

[3]*Department of Physics and Engineering Physics, Tulane University, New Orleans, Louisiana 70118, USA*

Corresponding emails: yubo.drzhang@mju.edu.cn, pzhang3@buffalo.edu, jsun@tulane.edu, perdew@tulane.edu

Abstract: In density functional theory, the SCAN (Strongly Constrained and Appropriately Normed) and r^{2}SCAN (regularized–restored SCAN) functionals significantly improve over GGA (Generalized Gradient Approximation) functionals such as PBE (Perdew–Burke–Ernzerhof) in predicting electronic, magnetic, and structural properties across various materials, including transition-metal compounds. However, there remain puzzling cases where SCAN/r^{2}SCAN underperform, such as in calculating the band structure of graphene, the magnetic moment of Fe, the potential energy curve of the Cr_2 molecule, and the bond length of VO_2. This research identifies a common characteristic among these challenging materials: non-compact covalent bonding through *s*-*s*, *p*-*p*, or *d*-*d* electron hybridization. While SCAN/r^{2}SCAN excel at capturing electron localization at local atomic sites, they struggle to accurately describe electron localization in non-compact covalent bonds, resulting in a biased improvement. To address this issue, we propose the r^{2}SCAN+V approach as a practical modification that improves accuracy across all the tested materials. The parameter V is 4 eV for metallic Fe, but substantially lower for the other cases. Our findings provide valuable insights for the future development of advanced functionals.

Significance statement:

To predict material properties, accurate but efficient approximations for the electronic exchange-correlation energy are needed. r^{2}SCAN satisfies many more exact conditions than PBE, and is more accurate in most cases, but there are puzzling cases where PBE is more accurate, including two-dimensional carbon, metallic iron, the chromium dimer, and solid vanadium dioxide. We show that these errors of r^{2}SCAN can be strongly reduced by making a one-parameter +V correction that localizes electrons near bond centers between nuclei, suggesting a correction of self-interaction error in non-compact covalent bonds. In such situations, r^{2}SCAN may provide much of the +U correction to PBE that localizes electrons near nuclei, and not enough of the compensating +V.

1. Introduction

Kohn-Sham density functional theory (DFT) [1] with the generalized gradient approximation (GGA) in the form of Perdew-Burke-Ernzerhof (PBE) [2] has long been the workhorse of condensed matter physics and materials science, but its reliability degrades for transition-metal materials. For example, PBE (even with spin-symmetry breaking [3]) frequently fails to capture the insulating characteristics of some Mott insulators. PBE's

primary limitation lies in its inadequate treatment of electron localization, giving rise to the self-interaction error (SIE), delocalization error, and strong correlation error [4,5,6]. A popular remedy is introducing an on-site Hubbard-U-like correction, which modifies the orbital-dependent potential (v_i) as $\Delta v_i = v_{\mathrm{DFT}+U} - v_{\mathrm{DFT}} = U(\frac{1}{2} - n_i)$ [7,8]. Here, Δv_i is negative for filled orbitals (with occupation $n_i = 1$) and positive for empty ones ($n_i = 0$). This corrective potential increases the energy splitting between occupied and unoccupied states, which explains its effectiveness in opening bandgaps of Mott insulators. In addition, the U potential enhances an on-site orbital's spatial localization by reducing SIE [9].

Although the U value can be determined from first principles [9], it is more commonly treated as an empirical parameter to reproduce some experimental quantities. Additionally, it has been observed that the GGA+U method can inadvertently suppress covalent hybridization between localized d orbitals and more dispersive p orbitals of anions [10,11]. For instance, in multiferroic $YMnO_3$, a minimum U value of 5 eV is required to open a bandgap; but this value is so large that it nearly suppresses p-d hybridization, rendering the d orbitals irrelevant for ferroelectric-ferromagnetic coupling [11].

Hybrid functionals, such as the Heyd-Scuseria-Ernzerhof (HSE) functional [12,13], demonstrate superior predictive accuracy for many semiconductors and insulators. However, HSE still faces accuracy challenges when applied to transition-metal materials, particularly metallic systems [14]. For instance, HSE06 incorrectly opens a bandgap in metallic $La_{2-x}Sr_xCuO_4$ [15], making this functional unsuitable for studying metal-insulator transitions. Additionally, the computational cost is prohibitively high for calculating large systems.

Introduced in 2015, the *Strongly Constrained and Appropriately Normed* (SCAN) meta-GGA functional [16] represents a remarkable advancement in DFT. Later, the r^{2}SCAN [17] was developed to improve the numerical stability. As general-purpose functionals, SCAN/r^{2}SCAN have demonstrated high accuracy across a broad spectrum of materials, including transition-metal compounds [3,18,19,20]. For example, in cuprate materials, SCAN not only accurately captures the pristine insulator and hole-doped metal [21], but also reliably predicts the emergence of a striped phase characterized by the coexistence of insulating and metallic regions [22]. The improved performance is primarily attributed to SCAN/r^{2}SCAN's ability to mitigate SIE [23,24]. Additionally, SCAN/r^{2}SCAN are able to recognize chemical bonds [25]—a critical feature for describing the pronounced anisotropy of d orbitals [11,24]. For instance, in $YMnO_3$, SCAN effectively characterizes various anisotropic orbitals, including highly localized non-bonding d orbitals, less localized bonding d orbitals, and dispersive sp orbitals [11]. These synergistic enhancements enable SCAN to open the bandgap of $YMnO_3$ without distorting the p-d hybridization. For many but not all transition metal compounds, SCAN and r^{2}SCAN can still be improved by +U corrections, but the needed U values are significantly smaller than for PBE [19]. Significant improvements without +U in the progression from local spin-density approximation (LSDA) [1] to the PBE GGA to the r^{2}SCAN meta-GGA have been found for the first three ionization energies of the 3d atoms [26], and for the oxidation energies of the ionically-bonded 3d transition-metal oxide solids [27].

SCAN and r^{2}SCAN also well capture the strong covalent bond energetics found in many main-group molecules at equilibrium [16,17], where strong hybridization of dispersive s and p orbitals can produce relatively *compact* bond orbital shapes. However, weak or stretched bonds and bonds involving localized d electrons are more prone to SIE in these functionals. A canonical example is the H_2^+ molecule [24], where delocalized s orbitals form a *compact* bond near the equilibrium position but gradually lose their compactness as the bond is stretched, due to the increasing orbital localization. The same effect at a weaker level is found in spin-symmetry broken H_2, for which r^{2}SCAN's accuracy diminishes as the bond transitions from the *compact* to the *non-compact* region (See Figure S7 in the Supplementary Material, and Section 3).

Despite SCAN/r^{2}SCAN's overall success, there are puzzling instances where they only match or underperform compared with PBE. A prominent example is SCAN's overestimation of the magnetic moments in metals, as demonstrated in a series of publications presented chronologically [28,29,30,31,32], predicting a value of 2.75 μ_B in elemental iron, which exceeds the experimentally measured 2.22 μ_B. In comparison, PBE offers a more accurate estimate of 2.20 μ_B. Additionally, SCAN faces accuracy issues in predicting the potential energy curve of the Cr_2 molecule, showing greater deviations than PBE [33]. SCAN/r^{2}SCAN also incorrectly open a bandgap for graphene [33] and inaccurately calculate the bond length of VO_2 [34].

From a shifting perspective, it is intriguing that PBE outperforms SCAN/r^{2}SCAN in these materials, despite PBE's more pronounced SIE. This observation mirrors a similar finding in calculating the ferroelectric properties of $BaTiO_3$, where the oldest LSDA reproduces the ferroelectric polarization with unexpected accuracy due to fortuitous error cancellation [35]. In calculating $BaTiO_3$, LSDA underestimates the geometric distortion while overestimating electronic polarizability. In contrast, PBE simultaneously overestimates both quantities, leading to a significant deviation in the calculated ferroelectric polarization. By comparison, SCAN accurately predicts the ferroelectricity for the correct reasons.

This work will reveal a common bonding characteristic in the computationally difficult materials (graphene, Cr_2, VO_2, and Fe): *non-compact* covalent bonding through *s*-*s*, *p*-*p*, or *d*-*d* electron hybridization. While r^{2}SCAN improves upon PBE in capturing electron localization at the *local atomic sites*, it falls short in accurately describing the *non-compact covalent bonds*, leading to a biased improvement and ultimately inferior overall performance. To address this limitation, we augment r^{2}SCAN with an inter-site potential V (i.e., r^{2}SCAN+V), inspired by the extended Hubbard model. The r^{2}SCAN+V method systematically improves calculations across all tested materials while being more computationally manageable than the original GGA+U+V approach [36,37,38,39,40].

For computational and other details, see the Supplementary Materials.

2. Graphene: non-compactness of π-bonds

Before addressing the computational issue, we briefly introduce the bonding interactions in graphene. Each carbon atom contributes three valence electrons to form sp^2 hybrid orbitals, which interact with those of two neighboring atoms, resulting in strong σ-bonds due to significant orbital overlap (see the inset of Figure 1a). The remaining electron occupies a delocalized p_z orbital, which hybridizes with two neighboring p_z orbitals, forming the weaker π-bonds that are responsible for the Dirac point. The relative isolation of the p_z orbitals naturally leads to certain localization characteristics, making the π-bonds relatively *non-compact* compared to the *compact* σ-bonds.

To induce a bandgap and magnetization in graphene, significant research efforts have been made, including contributions from the model Hamiltonian community. A study of the standard *Hubbard model* has established that Coulombic interactions between p_z orbitals are notably strong, approximating or even surpassing the threshold for spontaneous bandgap formation [41]. However, investigations of the *extended Hubbard model* [42,43] reveal that nonlocal inter-site interactions effectively screen the Coulombic interactions, thereby suppressing the bandgap formation [41,44,45].

Our r^{2}SCAN simulation, which incorporates spin-symmetry breaking, incorrectly predicts a bandgap (Figure 1a) by stabilizing local magnetic moments that are antiparallelly coupled on the bipartite lattice [33]. The emergence of magnetization, indicative of the Mott mechanism for bandgap formation [45,46], highlights

r^{2}SCAN's inaccuracy in balancing competition between the bonding and localization characteristics of the p_z orbitals. It turns out that the on-site localization characteristic is overestimated, which compromises the compactness of the π-bonds. Drawing on insights from the previous studies [41,44,45] using the *extended Hubbard model*, we consider the interaction V as defined in the Hamiltonian [36,42,43]:

$$H = t \sum_{\langle i,j\rangle,\sigma} (c^{\dagger}_{i,\sigma} c_{j,\sigma} + \text{h.c.}) + U \sum_{i} (n_{i,\uparrow} n_{i,\downarrow}) + V \sum_{\langle i,j\rangle} (n_i n_j)$$

where t is the kinetic energy, $c^{\dagger}_{i,\sigma}$ is the creation operator of an electron on site i with spin σ. The term U is the on-site energy that quantifies the energy penalty for double occupancy at the same atomic site i, signifying local electron-electron repulsion. The term V, on the other hand, represents the inter-site Coulombic interaction between electrons at neighboring sites i and j. When implementing V into DFT (i.e., DFT+V) [36,47,48], the corrective potential to the i-th site is $\Delta v_i = -V \sum_j n^{ij} P^{ji}$, where n_{ij} is the non-diagonal element of the occupation matrix between atomic sites i and j, and P^{ji} is a generalized projector capturing the non-diagonal nature of the occupation matrix. Clearly, a positive V stabilizes states that lead to finite n_{ij}, i.e., states with finite projections on both atoms of a nearest-neighbor couple. This behavior counteracts the tendency for localization on atomic states (a result of the +U correction) and allows the +V correction to account for electronic localization on inter-site orbitals.

The r^{2}SCAN+V calculation predicts both the bandgap and magnetization vanishing around $V \approx 2.0$ eV (Figure 1b). Additionally, the +V correction redistributes electrons from the p_z orbitals to the bond centers (see the insets of Figure 1b). Compared to PBE, r^{2}SCAN appears to include an implicit +U-like self-interaction correction to the p_z orbitals, whose effects on the bandgap and magnetization are counteracted by the explicit +V correction. These r^{2}SCAN+V results are consistent with the competing effects of +U and +V, as anticipated from the model Hamiltonian.

3. Cr_2 molecule with *d-d* and *s-s* hybridizations

The Cr_2 molecule features two distinct bonding distances in its potential energy curve: a short bond at 1.68 Å and an extended shelf around 2.4~3.0 Å. This unique characteristic makes Cr_2 an exemplary system for evaluating the predictive power of theories. Recent studies have revealed an intriguing puzzle: while many-body wavefunction methods have shown steady improvements over the years [49], the development of DFT seems to stray from the correct path, with predictions gradually worsening as one climbs Jacob's ladder [50] from GGA to meta-GGA to hybrid functionals (Figure 2a). Without a doubt, the computational difficulty arises from the bonding of intrinsically localized *d*-orbitals (and also *s-s* orbital hybridization, as discussed later), which contribute to the *non-compact* characteristics of the bond.

How does PBE achieve high accuracy in capturing the potential energy curve despite its significant SIE? To mitigate SIE in PBE, we adopt PBE+U_d and PBE+V_{dd} (where the subscripts *d* and *dd* indicate corrections on *d* orbitals) to improve the descriptions of the on-site region and inter-site interaction, respectively. However, the revised results become worse, as PBE+U_d excessively weakens the binding while PBE+V_{dd} overly strengthens it. When SIE is addressed simultaneously in both regions using PBE+U_d+V_{dd}, the good performance is restored, and the description of the short bond is even improved compared to PBE. These findings clearly indicate that +U and +V have opposing effects and must be considered together to improve upon PBE. However, determining precise U and V values is challenging, and the parameterization from the linear response approach [47,48] is unfortunately problematic for Cr_2 (Figure S2). Here, we fix U = 2.0 eV in PBE+U_d and V = 0.8 eV in PBE+V_{dd}; in PBE+U_d+V_{dd}, U is fixed at 2.0 eV, while V is fine-tuned to 2.2 eV to best reproduce the binding behavior.

With the aid of $+U$ and $+V$ simulations, we uncover the underlying reason for PBE's enigmatic effectiveness. The $+U_d$ method enhances electron localization on the Cr sites while depleting electrons from the bond center (Figure 2c). This redistribution reduces electronic screening of inter-atomic Coulombic repulsion, causing PBE+U_d to predict an underbinding curve. In contrast, the $+V_{dd}$ correction encourages electron accumulation on the bond (Figure 2d), leading to overbinding and reducing inter-atomic Coulombic repulsion. When applying $+U_d$ and $+V_{dd}$ simultaneously, the overall electron redistribution is relatively weak (Figure 2e), which explains the similar performance of PBE+U_d+V_{dd} and PBE. Therefore, PBE's high accuracy arises from its incidental balancing of electron delocalization errors in the site and bond regions.

Figure 2b presents the results using meta-GGAs. SCAN/r^{2}SCAN consistently underbind the molecule, similar to PBE+U_d, indicating that SCAN/r^{2}SCAN inherently enhance electron localization at atomic sites. Variants like r^{2}SCAN-L [51] and OFR2 [52], which are orbital-free meta-GGAs, show improved performance arising from better accounting of electronic screening effects [52]. However, further enhancements in describing non-compact electron localization are still needed, leading us to propose the r^{2}SCAN+V method. Interestingly, a parameter of V_{dd} = 0.8 eV in r^{2}SCAN+V achieves good agreement with experimental data, particularly in the short bonding region (1.4–2.4 Å). The shelf structure (starting at ~2.4 Å), originating from the hybridization of Cr-4*s* orbitals [49], is better reproduced when incorporating the inter-site potential V_{ss} = 0.8 eV onto neighboring *s* orbitals. This improvement highlights the *non-compactness* of *s*-*s* bonds, which are typically diffusive but can develop localization characteristics in stretched configurations, as observed in the shelf structure of Cr_2. The vital role of V_{ss} is also evidenced in the stretched H_2 molecule (Figure S7), where the 1*s* is the sole contributing orbital.

Strictly speaking, the V values should depend on bond lengths due to variations in electron localization. However, r^{2}SCAN+V with the V_{dd} and V_{ss} parameters tightly constrained around 0.8 eV can well reproduce the entire curve (Figure S3). The significant improvement, despite the small V parameters, not only highlights the effectiveness of the r^{2}SCAN+V method but also the critical role of functional nonlocality.

Although we identify electron localization in non-compact covalent bonds, we stress that it is not the density change itself but the functional's nonlocality that is most important for the predicted energetics. We confirmed this argument by comparing the binding energy curves from self-consistent r^{2}SCAN and from non-self-consistent r^{2}SCAN@r^{2}SCAN+V (i.e., r^{2}SCAN evaluated on the r^{2}SCAN+V's orbitals and density). The resulting binding energy curves are very similar (Figure S4), as expected, since density-driven errors of the energy [53] tend to be small [54] in the absence of large electron transfers between nuclear basins.

Figure S6 shows that the Cr_2 binding energy curve depends strongly on $V-U$ and weakly on U for a given $V-U$, suggesting that an empirical determination of U and V separately is not likely to be found.

For correlated wavefunction methods, the Cr_2 dimer is a notoriously difficult case of strong correlation [49]. Often spin-symmetry breaking [3,55,56] transforms strong correlation in a symmetric state into normal correlation in a symmetry-broken state that a reliable density functional can describe, but there is no proof that this must always yield correct energies. In Cr_2, the symmetric state is a singlet with zero spin polarization everywhere, and the broken-symmetry state is an antiferromagnetic dimer with a net spin up in one nuclear basin compensated by a net spin down in the other basin.

4. VO_2 with *d*-*d* hybridization

VO_2, a well-known strongly correlated material, has challenged DFT for decades. Our recent investigation

[34] identified a fundamental limitation of the popular functionals: none of LSDA, PBE, r^{2}SCAN, or HSE can accurately describe the vanadium-vanadium dimer length, and incorporating the on-site U correction may even worsen the predictions. Here, we reveal that VO_2 exhibits non-compact covalency involving localized d electrons, and r^{2}SCAN+V provides an effective improvement.

Figure 3a compares the dimer length predicted by various methods. PBE underestimates the length (2.53 Å), while r^{2}SCAN (2.66 Å) and HSE (2.70 Å) overestimate it. Incorporating a corrective U (2.0 eV) into PBE, a common strategy for studying VO_2, strongly overestimates the bond length (2.83 Å). The +U approach (i.e., PBE+U_d) leads to underbinding, as revealed by the electron redistribution pattern (Figure 3d): electrons accumulate on the atomic site while being depleted from the bonding region. As a result, the covalent bonding in the dimer is weakened, leading to bond length elongation. Further adding an inter-site V_{dd} term (i.e., PBE+U_d+V_{dd}) plays a counteracting role by drawing electrons back toward the bond center (Figure 3e). To match the experimental bond length, we fix U at 2.0 eV and identify the optimal V value of 2.2 eV.

We find that the PBE-based methods have notable limitations. First, PBE+U with a small U value of ~0.1 eV can well reproduce the experimental bond length (Figure S8), potentially giving the impression that PBE is nearly accurate for describing VO_2. However, this outcome is coincidental in VO_2, as observed for the Cr_2 molecule. Second, the PBE+U+V method, with the Hubbard parameters (U = 2.0 eV and V = 2.2 eV) deliberately chosen to reproduce the dimer length, introduces an adverse consequence: the bandgap is significantly overestimated (1.03 eV; see Figure 3b), which is atypical for local and semilocal functionals.

In contrast, the r^{2}SCAN+V method addresses both on-site and on-bond electron localization with simplified parameterization. Using a V value of 0.5 eV, r^{2}SCAN+V accurately reproduces the bond length (Figure 3a) while yielding a reasonable bandgap (Figure 3b). The mechanism is again revealed by electron accumulation in the nonlocal region (Figure 3f).

While the above simulations have adopted a spin-symmetry-breaking (SSB) treatment, VO_2 has a spin-singlet ground state for the vanadium dimer. SSB has been criticized [57] due to the emergence of local magnetic moments (Figure 3c). However, we discuss three key justifications for the SSB treatment. First, several authors of this work have established that SSB is, in general, far more revealing than its spin-restricting counterpart [55,56,58]. SSB can reveal dynamic but slow spin fluctuations. Second, the SSB treatment of VO_2, which leads to an electron deficiency at the bond, becomes physically accurate when combined with a positive inter-site V, as it mitigates the deficiency by redistributing electrons back to the bond. In contrast, the spin-restricting treatment [57], which already causes electron over-accumulation on the bond, worsens the problem when combined with the corrective V method. For instance, PBE+V (V = 2 eV) under spin-restricting treatment exacerbates the over-binding problem, resulting in an excessively short bond length of 2.46 Å [57]. Finally, the broken symmetry introduced by SSB can be restored afterward [59], ensuring the correct wavefunction symmetry.

5. Fe with *d-d* covalent bonding and hidden antiferromagnetism

SCAN's applicability to transition-metal materials was initially questioned in elemental Fe, revealing an overestimation of magnetic moment [28,29,30,31,32]. This issue is closely related to the behavior of the iso-orbital indicator (α) in the radial region $0.6 \le r \le 1.2$ Bohr, as first identified in Ref. [60] (which suggested that a flattening of the exchange interpolation function $f_x(\alpha)$ near $\alpha = 1$ would yield a smaller and more realistic magnetic moment). This issue in Fe invites comparisons with graphene, Cr_2, and VO_2. Here, we reveal that Fe also demonstrates non-compact covalent bonding, which occurs only between partial atomic shells and is

concealed within a metallic background. To provide a comprehensive analysis, we systematically examine the bonding characteristics of four elemental metals—Cr, Fe, Co, and Ni—excluding Mn due to its large unit cell, using the projected Crystal Orbital Hamilton Populations (pCOHP) method [61,62]. As shown in Figure 4a, the valence bands of Cr are predominantly characterized by bonding states, with an increasing incorporation of antibonding states as we progress to Fe, Co, and Ni. This trend is quantitatively captured by the integrated pCOHP (Figure 4b), where the monotonically decreasing values reflect progressively weaker covalent bonding among the four materials.

Whereas Cr has a static spiral spin-density wave, we adopt a collinear antiferromagnetic model for simplicity. Calculations reveal that Cr exhibits the most significant covalency. Fe also demonstrates considerable covalency and features an antiferromagnetic coupling between its t_{2g} orbitals [63], concealed within a ferromagnetic background. The covalency and antiferromagnetism in Cr and Fe, associated with direct overlap of adjacent *d* orbitals, may reflect underlying physics similar to that observed in graphene, Cr_2, and VO_2. Indeed, the electron redistribution provides straightforward evidence: an inter-site V potential accumulates electrons on the shortest bonds in Cr and Fe (Figures 4c and 4d), but the pattern is absent in Co and Ni (Figure S10).

Having established the covalency feature in Cr and Fe, we calculate their magnetic moments using the r^{2}SCAN+V method with varying V values, as shown in Figure 5a. Without the +V correction, r^{2}SCAN alone predicts a magnetic moment of 2.12 μ_B for Cr, significantly higher than the experimental value of 0.51 μ_B [64]. For Fe, the result is similarly overestimated at 2.95 μ_B compared to the experimental result of 2.22 μ_B [65]. The +V correction effectively reduces the magnetic moments: $V \approx 2.0$ eV for Cr and $V \approx 4.0$ eV for Fe, yielding results that closely match experimental values. In contrast, the +V correction for Co and Ni has a negligible effect or slightly increases the magnetic moments, suggesting that this correction may not be applicable. The small overestimation of Ni's moment by r^{2}SCAN likely originates from other factors and warrants further investigation.

The optimal V values in r^{2}SCAN+V, which are chosen to best reproduce specific experimental quantities, show considerable variation across the tested materials. For example, $V_{pp} \geq 2$ eV for graphene, $V_{dd} = V_{ss} = 0.8$ eV for the Cr_2 molecule, $V_{dd} = 0.5$ eV for VO_2, $V_{dd} = 2$ eV for Cr, and $V_{dd} = 4$ eV for Fe. Overall, the V values are relatively small (except for Fe). On one hand, the excessively large values for Cr and Fe may be artifacts associated with *d*-orbital anisotropy, as revealed by orbital-resolved DFT+U simulations [10]. On the other hand, the material dependence is also closely tied to varying electronic screenings, highlighting the need for an advanced DFT functional capable of accurately capturing these subtleties. As a demonstration, Figure 5b compares the performance of various functionals, roughly organized by increasing magnetic moments. Among these, the OFR2 functional [52] and the r^{2}SCAN-L functional [51], which are well suited to the perfect long-range screening in a metal, predict smaller magnetic moments. Thus, the magnetic moments serve as an informative indicator of how effectively DFT functionals describe the non-compact bonds.

6. Discussion and Summary

We have proposed a possible way to understand the successes and puzzling failures of the non-empirical PBE and SCAN/r^{2}SCAN density functionals. The studied materials of graphene, Cr_2 molecule, VO_2, Cr, and Fe demonstrate notable non-compact covalent bonding through *s-s*, *p-p*, or *d-d* orbital hybridization, which accumulates electrons on the bond centers. At the same time, the involved *s*, *p*, or *d* orbitals exhibit electron localization around the atomic centers, either due to intrinsic localization or as a result of the stretched configuration. It is crucial for DFT functionals to simultaneously account for electrons at local atomic sites and within non-compact bonds. PBE, while suffering from electron delocalization errors in both regions,

accidentally strikes a balance in describing these materials (Figure 6a). In contrast, r^{2}SCAN enhances the localization of site-centered electrons more effectively than PBE, but it does not equally improve the localization of bond-centered electrons in non-compact bonds (Figure 6b). Such biased improvement compromises r^{2}SCAN's accuracy.

The original GGA+U+V method [36,37,38,39,40] could potentially enhance electron localization in both regions, yet it faces practical difficulties in determining U and V values in the tested materials. The r^{2}SCAN+V approach simplifies parameter management and effectively resolves the accuracy challenges for all tested materials with typically small V parameters. Future revisions of r^{2}SCAN may need to better account for this kind of inter-site effect. Whether this can be achieved within or only beyond the computationally-efficient meta-GGA functional form, in particular when including both kinetic energy density and Laplacian of electron density as its ingredients [66], and without material-dependent fitted parameters, remains to be seen. Fully non-local and thus less computationally efficient self-interaction corrections [5,67] that make a functional exact for all one-electron densities require a unitary transformation to localized orbitals, including covalent-bond orbitals. A future refinement of Refs. [5,67] that does no harm to r^{2}SCAN accuracy (in the sense that the just-developed LSIC-α does no harm to LSDA accuracy) might boost the accuracy of r^{2}SCAN for the systems studied here, while satisfying an 18th exact constraint. Uncorrected SCAN and r^{2}SCAN are only approximately self-interaction-free, and only for compact one-electron densities [68,69].

The behavior identified here reflects intrinsic limitations of SCAN-like meta-GGAs. While these functionals satisfy all 17 exact constraints accessible to a computationally efficient meta-GGA, they cannot be exact for all one-electron densities and are instead normed to a single compact orbital shape—the spherical exponential density of a one-electron atom or ion. As a result, SCAN-like functionals are much more accurate for compact one-electron densities than for non-compact ones, explaining their excellent performance for on-site localization and their failures for non-compact bond-centered or inter-site localization, as exemplified by stretched H_2^+ [24]. The use of the iso-orbital indicator α and kinetic-energy density ensures correct one-electron correlation but cannot recover the fully nonlocal exchange needed for non-compact densities, making improvements over GGAs statistical rather than systematic. Additional challenges arise in metals, where long-range screening shortens the exchange–correlation hole in ways not captured by standard meta-GGA ingredients. These observations suggest that further progress will require increased conceptual freedom, for example through refined gradient expansions, additional semilocal ingredients such as the density Laplacian, or controlled nonlocal corrections, to achieve more systematic improvements while retaining computational efficiency.

Meta-GGA functionals, similar to SCAN or its modifications, are under active development. Recently, the Lebeda-Aschebrock-Kümmel (LAK) meta-GGA [70,71] demonstrated remarkable accuracy in predicting atomization energies, bond lengths, bandgaps, and capturing weak interactions near equilibrium. To address the over-magnetization issue of SCAN, a modification called mSCAN [72] "*provides a solution that satisfies the most pressing desiderata for density functional approximations in ferromagnetic, antiferromagnetic, and noncollinear states*". While these functionals offer significant improvements in many areas, their accuracy for certain cases, such as the Cr_2 molecule (Figure S5), still requires further refinement.

Acknowledgments

YZ is supported by the Startup Grant of Minjiang University (30804326) and the Natural Science Foundation of Fujian Province (Grant No. 2023J02032). TL and JS acknowledge the U.S. DOE, Office of

Science, Basic Energy Sciences (BES), Grant No. DE-SC0014208. RM was supported by DMR-2426275. TL was supported by the U.S. National Science Foundation under Grant No. CHE-2533416 to JPP and JS. JPP was supported by the U.S. National Science Foundation under Grant No. DMR-2426275, and by the U.S. Department of Energy. Basic Energy Sciences, under Grant. No. DE-SC0018331.

Conflict of Interest

The authors have no conflicts to disclose.

Data availability

The data that support the findings of this study are available within the article and supplementary materials.

References

[1] W. Kohn, L. J. Sham, *Self-Consistent Equations Including Exchange and Correlation Effects*. Physical Review. 140, A1133 (1965).

[2] John P. Perdew, Kieron Burke, Matthias Ernzerhof, *Generalized Gradient Approximation Made Simple*. Physical Review Letters. 77, 3865 (1996).

[3] Alex Zunger, Jia-Xin Xiong, John P. Perdew, *Symmetry breaking transforms strong to normal correlation and false metals to true insulators*. arXiv preprint arXiv:2512.18236, (2025).

[4] Kyle R. Bryenton, Adebayo A. Adeleke, Stephen G. Dale, Erin R. Johnson, *Delocalization error: The greatest outstanding challenge in density-functional theory*. WIREs Computational Molecular Science. 13, e1631 (2022).

[5] John P Perdew, Alex Zunger, *Self-interaction correction to density-functional approximations for many-electron systems*. Physical Review B. 23, 5048 (1981).

[6] Aron J. Cohen, Paula Mori-Sánchez, Weitao Yang, *Insights into Current Limitations of Density Functional Theory*. Science. 321, 792 (2008).

[7] Vladimir I. Anisimov, Jan Zaanen, Ole K. Andersen, *Band theory and Mott insulators: Hubbard U instead of Stoner I*. Physical Review B. 44, 943 (1991).

[8] I. Anisimov Vladimir, F. Aryasetiawan, A. I. Lichtenstein, *First-principles calculations of the electronic structure and spectra of strongly correlated systems: the LDA+U method*. Journal of Physics: Condensed Matter. 9, 767 (1997).

[9] Matteo Cococcioni, Stefano de Gironcoli, *Linear response approach to the calculation of the effective interaction parameters in the LDA+U method*. Physical Review B. 71, 035105 (2005).

[10] Eric Macke, Iurii Timrov, Nicola Marzari, Lucio Colombi Ciacchi, *Orbital-Resolved DFT+U for Molecules and Solids*. Journal of Chemical Theory and Computation. 20, 4824 (2024).

[11] Da Ke, Jianwei Sun, Yubo Zhang, *Accurate DFT Simulation of Complex Functional Materials: Synergistic Enhancements Achieved by SCAN meta-GGA*. The Journal of Chemical Physics. 162, 014107 (2024).

[12] Jochen Heyd, Gustavo E. Scuseria, Matthias Ernzerhof, *Hybrid functionals based on a screened Coulomb potential*. The Journal of Chemical Physics. 118, 8207 (2003).

[13] Jochen Heyd, Gustavo E. Scuseria, Matthias Ernzerhof, *Erratum: "Hybrid functionals based on a screened Coulomb potential" [J. Chem. Phys. 118, 8207 (2003)]*. The Journal of Chemical Physics. 124, 219906 (2006).

[14] Weiwei Gao, Tesfaye A. Abtew, Tianyi Cai, Yi-Yang Sun, Shengbai Zhang, Peihong Zhang, *On the applicability of hybrid functionals for predicting fundamental properties of metals*. Solid State Communications. 234-235, 10 (2016).

[15] Kanun Pokharel, Christopher Lane, James W. Furness, Ruiqi Zhang, Jinliang Ning, Bernardo Barbiellini, Robert S. Markiewicz, Yubo Zhang, Arun Bansil, Jianwei Sun, *Sensitivity of the electronic and magnetic structures of cuprate superconductors to density functional approximations*. npj Computational Materials. 8,

31 (2022).

[16] Jianwei Sun, Adrienn Ruzsinszky, John P Perdew, *Strongly Constrained and Appropriately Normed Semilocal Density Functional*. Physical Review Letters. 115, 036402 (2015).

[17] James W Furness, Aaron D Kaplan, Jinliang Ning, John P Perdew, Jianwei Sun, *Accurate and Numerically Efficient r^{2}SCAN Meta-Generalized Gradient Approximation*. The Journal of Physical Chemistry Letters. 11, 8208 (2020).

[18] Yubo Zhang, Akilan Ramasamy, Kanun Pokharel, Manish Kothakonda, Bing Xiao, James W. Furness, Jinliang Ning, Ruiqi Zhang, Jianwei Sun, *Advances and Challenges of SCAN and r^{2}SCAN Density Functionals in Transition-Metal Compounds*. WIREs Computational Molecular Science. 15, e70007 (2025).

[19] S. Swathilakshmi, R. Devi, G. Sai Gautam, *Performance of the r^{2}SCAN Functional in Transition Metal Oxides*. Journal of Chemical Theory and Computation. 19, 4202 (2023).

[20] J. Sun, R. C. Remsing, Y. Zhang, Z. Sun, A. Ruzsinszky, H. Peng, Z. Yang, A. Paul, U. Waghmare, X. Wu, M. L. Klein, J. P. Perdew, *Accurate first-principles structures and energies of diversely bonded systems from an efficient density functional*. Nature Chemistry. 8, 831 (2016).

[21] James W. Furness, Yubo Zhang, Christopher Lane, Ioana Gianina Buda, Bernardo Barbiellini, Robert S. Markiewicz, Arun Bansil, Jianwei Sun, *An accurate first-principles treatment of doping-dependent electronic structure of high-temperature cuprate superconductors*. Communications Physics. 1, 11 (2018).

[22] Yubo Zhang, Christopher Lane, James W Furness, Bernardo Barbiellini, John P Perdew, Robert S Markiewicz, Arun Bansil, Jianwei Sun, *Competing stripe and magnetic phases in the cuprates from first principles*. Proceedings of the National Academy of Sciences of the USA. 117, 68 (2020).

[23] Yubo Zhang, James W. Furness, Bing Xiao, Jianwei Sun, *Subtlety of TiO_2 phase stability: Reliability of the density functional theory predictions and persistence of the self-interaction error*. The Journal of Chemical Physics. 150, 014105 (2019).

[24] Yubo Zhang, James Furness, Ruiqi Zhang, Zhi Wang, Alex Zunger, Jianwei Sun, *Symmetry-breaking polymorphous descriptions for correlated materials without interelectronic U*. Physical Review B. 102, 045112 (2020).

[25] Jianwei Sun, Bing Xiao, Yuan Fang, Robin Haunschild, Pan Hao, Adrienn Ruzsinszky, Gábor I. Csonka, Gustavo E. Scuseria, John P. Perdew, *Density Functionals that Recognize Covalent, Metallic, and Weak Bonds*. Physical Review Letters. 111, 106401 (2013).

[26] Rohan Maniar, Priyanka B. Shukla, J. Karl Johnson, Koblar A. Jackson, John P. Perdew, *Atomic ionization: sd energy imbalance and Perdew–Zunger self-interaction correction energy penalty in 3d atoms*. Proceedings of the National Academy of Sciences. 122, e2418305122 (2025).

[27] Harshan Reddy Gopidi, Ruiqi Zhang, Yanyong Wang, Abhirup Patra, Jianwei Sun, Adrienn Ruzsinszky, John P Perdew, Pieremanuele Canepa, *Reducing Self-Interaction Error in Transition-Metal Oxides with Different Exact-Exchange Fractions for Energy and Density*. arXiv preprint arXiv:2506.20635, (2025).

[28] Eric B. Isaacs, Chris Wolverton, *Performance of the strongly constrained and appropriately normed density functional for solid-state materials*. Physical Review Materials. 2, 063801 (2018).

[29] Subrata Jana, Abhilash Patra, Prasanjit Samal, *Assessing the performance of the Tao-Mo semilocal density functional in the projector-augmented-wave method*. The Journal of Chemical Physics. 149, 044120 (2018).

[30] Aldo H. Romero, Matthieu J. Verstraete, *From one to three, exploring the rungs of Jacob's ladder in magnetic alloys*. The European Physical Journal B. 91, 193 (2018).

[31] M. Ekholm, D. Gambino, H. J. M. Jönsson, F. Tasnádi, B. Alling, I. A. Abrikosov, *Assessing the SCAN functional for itinerant electron ferromagnets*. Physical Review B. 98, 094413 (2018).

[32] Yuhao Fu, David J. Singh, *Applicability of the Strongly Constrained and Appropriately Normed Density Functional to Transition-Metal Magnetism*. Physical Review Letters. 121, 207201 (2018).

[33] Yubo Zhang, Wenqing Zhang, David J. Singh, *Localization in the SCAN meta-generalized gradient approximation functional leading to broken symmetry ground states for graphene and benzene*. Physical Chemistry Chemical Physics. 22, 19585 (2020).

[34] Yubo Zhang, Da Ke, Junxiong Wu, Chutong Zhang, Lin Hou, Baichen Lin, Zuhuang Chen, John P Perdew, Jianwei Sun, *Challenges for density functional theory in simulating metal-metal singlet bonding: A case study of dimerized VO_2*. J Chem Phys. 160, 134101 (2024).

[35] Yubo Zhang, Jianwei Sun, John P. Perdew, Xifan Wu, *Comparative first-principles studies of prototypical ferroelectric materials by LDA, GGA, and SCAN meta-GGA*. Physical Review B. 96, 035143 (2017).

[36] Vivaldo Leiria Campo, Matteo Cococcioni, *Extended DFT+U+V method with on-site and inter-site electronic interactions*. Journal of Physics: Condensed Matter. 22, 055602 (2010).

[37] Heather J. Kulik, Nicola Marzari, *Transition-metal dioxides: A case for the intersite term in Hubbard-model functionals*. The Journal of Chemical Physics. 134, 094103 (2011).

[38] Matteo Cococcioni, Nicola Marzari, *Energetics and cathode voltages of LiMPO4 olivines (M = Fe, Mn) from extended Hubbard functionals*. Physical Review Materials. 3, 033801 (2019).

[39] Iurii Timrov, Francesco Aquilante, Matteo Cococcioni, Nicola Marzari, *Accurate Electronic Properties and Intercalation Voltages of Olivine-Type Li-Ion Cathode Materials from Extended Hubbard Functionals*. PRX Energy. 1, 033003 (2022).

[40] G. Gebreyesus, Lorenzo Bastonero, Michele Kotiuga, Nicola Marzari, Iurii Timrov, *Understanding the role of Hubbard corrections in the rhombohedral phase of $BaTiO_3$*. Physical Review B. 108, 235171 (2023).

[41] M. Schüler, M. Rösner, T. O. Wehling, A. I. Lichtenstein, M. I. Katsnelson, *Optimal Hubbard Models for Materials with Nonlocal Coulomb Interactions: Graphene, Silicene, and Benzene*. Physical Review Letters. 111, 036601 (2013).

[42] J. Hubbard, *Electron correlations in narrow energy bands - IV. The atomic representation*. Proceedings of the Royal Society of London. Series A. Mathematical and Physical Sciences. 285, 542 (1965).

[43] J. Hubbard, *Electron correlations in narrow energy bands V. A perturbation expansion about the atomic limit*. Proceedings of the Royal Society of London. Series A. Mathematical and Physical Sciences. 296, 82 (1967).

[44] M. V. Ulybyshev, P. V. Buividovich, M. I. Katsnelson, M. I. Polikarpov, *Monte Carlo Study of the Semimetal-Insulator Phase Transition in Monolayer Graphene with a Realistic Interelectron Interaction Potential*. Physical Review Letters. 111, 056801 (2013).

[45] M. Schüler, E. G. C. P. van Loon, M. I. Katsnelson, T. O. Wehling, *First-order metal-insulator transitions in the extended Hubbard model due to self-consistent screening of the effective interaction*. Physical Review B. 97, 165135 (2018).

[46] Joaquín E. Drut, Timo A. Lähde, *Is Graphene in Vacuum an Insulator?* Physical Review Letters. 102, 026802 (2009).

[47] Iurii Timrov, Nicola Marzari, Matteo Cococcioni, *Self-consistent Hubbard parameters from density-functional perturbation theory in the ultrasoft and projector-augmented wave formulations*. Physical Review B. 103, 045141 (2021).

[48] Iurii Timrov, Nicola Marzari, Matteo Cococcioni, *HP – A code for the calculation of Hubbard parameters using density-functional perturbation theory*. Computer Physics Communications. 279, 108455 (2022).

[49] Henrik R. Larsson, Huanchen Zhai, C. J. Umrigar, Garnet Kin-Lic Chan, *The Chromium Dimer: Closing a Chapter of Quantum Chemistry*. Journal of the American Chemical Society. 144, 15932 (2022).

[50] John P. Perdew, Karla Schmidt, *Jacob's ladder of density functional approximations for the exchange-correlation energy*. AIP Conference Proceedings. 577, 1 (2001).

[51] Daniel Mejía-Rodríguez, S. B. Trickey, *Meta-GGA performance in solids at almost GGA cost*. Physical Review B. 102, 121109 (2020).

[52] Aaron D. Kaplan, John P. Perdew, *Laplacian-level meta-generalized gradient approximation for solid and liquid metals*. Physical Review Materials. 6, 083803 (2022).

[53] Min-Cheol Kim, Eunji Sim, Kieron Burke, *Understanding and reducing errors in density functional calculations*. Physical Review Letters. 111, 073003 (2013).

[54] Aaron D. Kaplan, Chandra Shahi, Raj K. Sah, Pradeep Bhetwal, Bikash Kanungo, Vikram Gavini, John P. Perdew, *How Does HF-DFT Achieve Chemical Accuracy for Water Clusters?* Journal of Chemical Theory and Computation. 20, 5517 (2024).

[55] John P Perdew, Adrienn Ruzsinszky, Jianwei Sun, Niraj K Nepal, Aaron D Kaplan, *Interpretations of ground-state symmetry breaking and strong correlation in wavefunction and density functional theories*. Proceedings of the National Academy of Sciences of the USA. 118, e2017850 (2021).

[56] John P. Perdew, *SCAN meta-GGA, strong correlation, symmetry breaking, self-interaction correction, and semi-classical limit in density functional theory: Hidden connections and beneficial synergies?* APL

Computational Physics. 1, 010903 (2025).

[57] Lea Haas, Peter Mlkvik, Nicola A. Spaldin, Claude Ederer, *Incorporating static intersite correlation effects in vanadium dioxide through DFT+V*. Physical Review Research. 6, 043177 (2024).

[58] Rohan Maniar, Kushantha P. K. Withanage, Chandra Shahi, Aaron D. Kaplan, John P. Perdew, Mark R. Pederson, *Symmetry breaking and self-interaction correction in the chromium atom and dimer*. The Journal of Chemical Physics. 160, 144301 (2024).

[59] J. A. Sheikh, J. Dobaczewski, P. Ring, L. M. Robledo, C. Yannouleas, *Symmetry restoration in mean-field approaches*. Journal of Physics G: Nuclear and Particle Physics. 48, 123001 (2021).

[60] Daniel Mejía-Rodríguez, S. B. Trickey, *Analysis of over-magnetization of elemental transition metal solids from the SCAN density functional*. Physical Review B. 100, 041113 (2019).

[61] Richard Dronskowski, Peter E. Bloechl, *Crystal orbital Hamilton populations (COHP): energy-resolved visualization of chemical bonding in solids based on density-functional calculations*. The Journal of Physical Chemistry. 97, 8617 (1993).

[62] Volker L. Deringer, Andrei L. Tchougréeff, Richard Dronskowski, *Crystal Orbital Hamilton Population (COHP) Analysis As Projected from Plane-Wave Basis Sets*. The Journal of Physical Chemistry A. 115, 5461 (2011).

[63] Y. O. Kvashnin, R. Cardias, A. Szilva, I. Di Marco, M. I. Katsnelson, A. I. Lichtenstein, L. Nordström, A. B. Klautau, O. Eriksson, *Microscopic Origin of Heisenberg and Non-Heisenberg Exchange Interactions in Ferromagnetic bcc Fe*. Physical Review Letters. 116, 217202 (2016).

[64] A. Arrott, S. A. Werner, H. Kendrick, *Neutron-Diffraction Study of Dilute Chromium Alloys with Iron*. Physical Review. 153, 624 (1967).

[65] H. Danan, A. Herr, A. J. P. Meyer, *New Determinations of the Saturation Magnetization of Nickel and Iron*. Journal of Applied Physics. 39, 669 (1968).

[66] Akilan Ramasamy, Lin Hou, Jorge Vega Bazantes, Tom J. P. Irons, Andrew M. Wibowo-Teale, Timo Lebeda, Jianwei Sun, *Tackling the one-electron self-interaction error within the semilocal density functional framework*. Physical Review B. 112, L161112 (2025).

[67] Mark R. Pederson, Adrienn Ruzsinszky, John P. Perdew, *Communication: Self-interaction correction with unitary invariance in density functional theory*. The Journal of Chemical Physics. 140, 121103 (2014).

[68] Chandra Shahi, Puskar Bhattarai, Kamal Wagle, Biswajit Santra, Sebastian Schwalbe, Torsten Hahn, Jens Kortus, Koblar A. Jackson, Juan E. Peralta, Kai Trepte, Susi Lehtola, Niraj K. Nepal, Hemanadhan Myneni, Bimal Neupane, Santosh Adhikari, Adrienn Ruzsinszky, Yoh Yamamoto, Tunna Baruah, Rajendra R. Zope, John P. Perdew, *Stretched or noded orbital densities and self-interaction correction in density functional theory*. The Journal of Chemical Physics. 150, 174102 (2019).

[69] Lin Hou, Cody Woods, Yanyong Wang, Jorge Vega Bazantes, Ruiqi Zhang, Shimin Zhang, Erik Alfredo Perez Caro, Yuan Ping, Timo Lebeda, Jianwei Sun, *Artificial Symmetry Breaking by Self-Interaction Error*. arXiv preprint arXiv:2506.20662, (2025).

[70] Timo Lebeda, Thilo Aschebrock, Stephan Kümmel, *Balancing the Contributions to the Gradient Expansion: Accurate Binding and Band Gaps with a Nonempirical Meta-GGA*. Physical Review Letters. 133, 136402 (2024).

[71] Timo Lebeda, Stephan Kümmel, *Meta-GGA that describes weak interactions in addition to bond energies and band gaps*. Physical Review B. 111, 155133 (2025).

[72] Jacques K. Desmarais, Alessandro Erba, Giovanni Vignale, Stefano Pittalis, *Meta-Generalized Gradient Approximation Made Magnetic*. Physical Review Letters. 134, 106402 (2025).

[73] Sean M. Casey, Doreen G. Leopold, *Negative ion photoelectron spectroscopy of chromium dimer*. The Journal of Physical Chemistry. 97, 816 (1993).

[74] V. Eyert, *The metal-insulator transitions of VO_2: A band theoretical approach*. Annalen der Physik. 514, 650 (2002).

[75] H. P. Myers, Willie Sucksmith, *The spontaneous magnetization of cobalt*. Proceedings of the Royal Society of London. Series A. Mathematical and Physical Sciences. 207, 427 (1951).

Figure captions

Figure 1. Electronic properties of graphene. (a) Bands derived from the p_z orbitals. The calculations use r^{2}SCAN, with or without spin-symmetry breaking. The inset illustrates the σ- and π-bonds. (b) Bandgap and magnetic moment as functions of V values in r^{2}SCAN+V. The insets illustrate electron redistribution among the σ- and π-bonds induced by the $+V$ (2 eV) correction, represented as $\Delta n = n^{\mathrm{r^2SCAN}+V} - n^{\mathrm{r^2SCAN}}$. The upper inset is a 3D plot, while the lower inset provides a 2D cross-section of a C-C bond perpendicular to the lattice plane. Red and blue lines indicate electron depletion and accumulation, respectively.

Figure 2. Electronic properties of the Cr_2 molecule. (a,b) Potential energy curve predicted by various methods. The experimental results are cited from [73]. In subplot (b), while V_{dd} is applied at all bond lengths, V_{ss} is only applied to the shelf structure starting at 2.4 Å. (c) Patterns of electron redistribution due to the additional corrections, represented as $\Delta n = n^{\mathrm{PBE}+U_d(2\mathrm{eV})} - n^{\mathrm{PBE}}$. (d) $\Delta n = n^{\mathrm{PBE}+V_{dd}(0.8\mathrm{eV})} - n^{\mathrm{PBE}}$. (e) $\Delta n = n^{\mathrm{PBE}+U_d(2\mathrm{eV})+V_{dd}(2.2\mathrm{eV})} - n^{\mathrm{PBE}}$. (f) $\Delta n = n^{\mathrm{r^2SCAN}+V_{dd}(0.8\mathrm{eV})} - n^{\mathrm{r^2SCAN}}$. Red and blue lines indicate electron depletion and accumulation, respectively. The plots of (c) to (f) correspond to the length of 1.68 Å.

Figure 3. Properties of VO_2. (a) Length of vanadium-vanadium dimer. Note that the lattice constants are fixed to their experimental values due to technical constraints, and only the ionic positions are optimized. The experimental value is 2.62 Å [74]. (b) Bandgap. (c) Local magnetic moments. (d) Redistribution of electron density, $\Delta n = n^{\mathrm{PBE}+U(2\mathrm{eV})} - n^{\mathrm{PBE}}$. The $+U$ correction induces inhomogeneous electron redistribution, causing accumulation in non-bonded t_2 orbitals and depletion from directional V-O bonds, while overall resulting in electron accumulation at the vanadium site. (e) $\Delta n = n^{\mathrm{PBE}+U(2\mathrm{eV})+V(2.2\mathrm{eV})} - n^{\mathrm{PBE}+U(2\mathrm{eV})}$. (f) $\Delta n = n^{\mathrm{r^2SCAN}+V(0.5\mathrm{eV})} - n^{\mathrm{r^2SCAN}}$. Red and blue colors denote electron depletion and accumulation, respectively.

Figure 4. Bonding properties of transition metals. (a) The negative values of *projected Crystal orbital Hamilton populations*, –pCOHP. The PBE functional is used here; r^{2}SCAN results are presented in Figure S9. (b) Integrated value, –IpCOHP. (c) Electron redistribution in Cr, $\Delta n = n^{\mathrm{r^2SCAN}+V(2\mathrm{eV})} - n^{\mathrm{r^2SCAN}}$. (d) Electron redistribution for Fe, $\Delta n = n^{\mathrm{r^2SCAN}+V(4\mathrm{eV})} - n^{\mathrm{r^2SCAN}}$. The V potential is on the 3d orbitals. Red and blue isosurfaces/lines denote electron depletion and accumulation, respectively.

Figure 5. Magnetic moment of transition metals. (a) Simulation performed using r^{2}SCAN+V with varying V values. (b) Simulations conducted with various functionals, abbreviated as follows: **L** for LSDA, **P** for PBE, **O** for OFR2, **RL** for r^{2}SCAN-L, **S** for SCAN, **R** for r^{2}SCAN, and **H** for HSE06. VASP and Quantum Espresso are used for cross-checking, but the OFR2 functional is unavailable in Quantum Espresso. Experimental values for local magnetic moments are taken from Cr [64], Fe [65], Co [75], and Ni [65].

Figure 6. Sketch of the site-centered and bond-centered electron localization. (a) PBE's superior performance arises from coincidental error cancellation, despite pronounced delocalization errors in both site- and bond-centered regions. (b) r^{2}SCAN's underperformance results from its biased improvement at atomic sites.

Figures

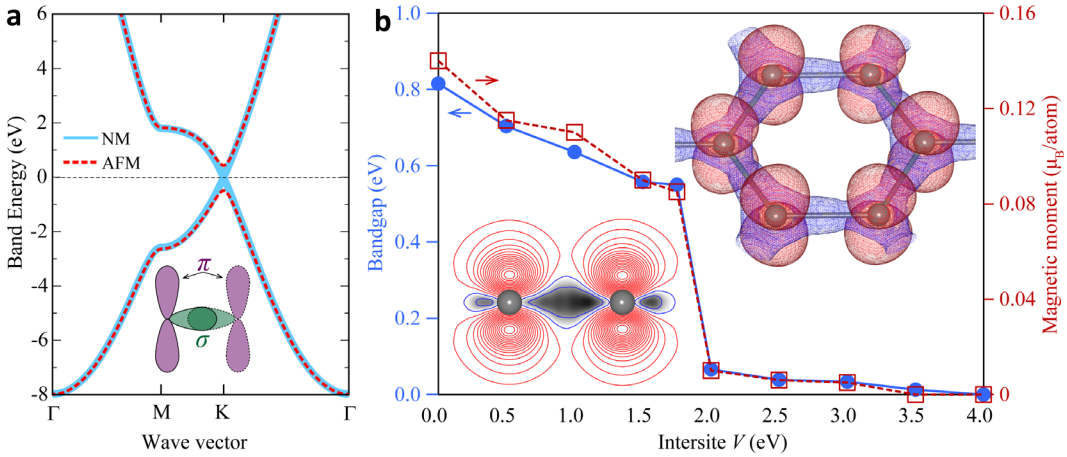

Figure 1.

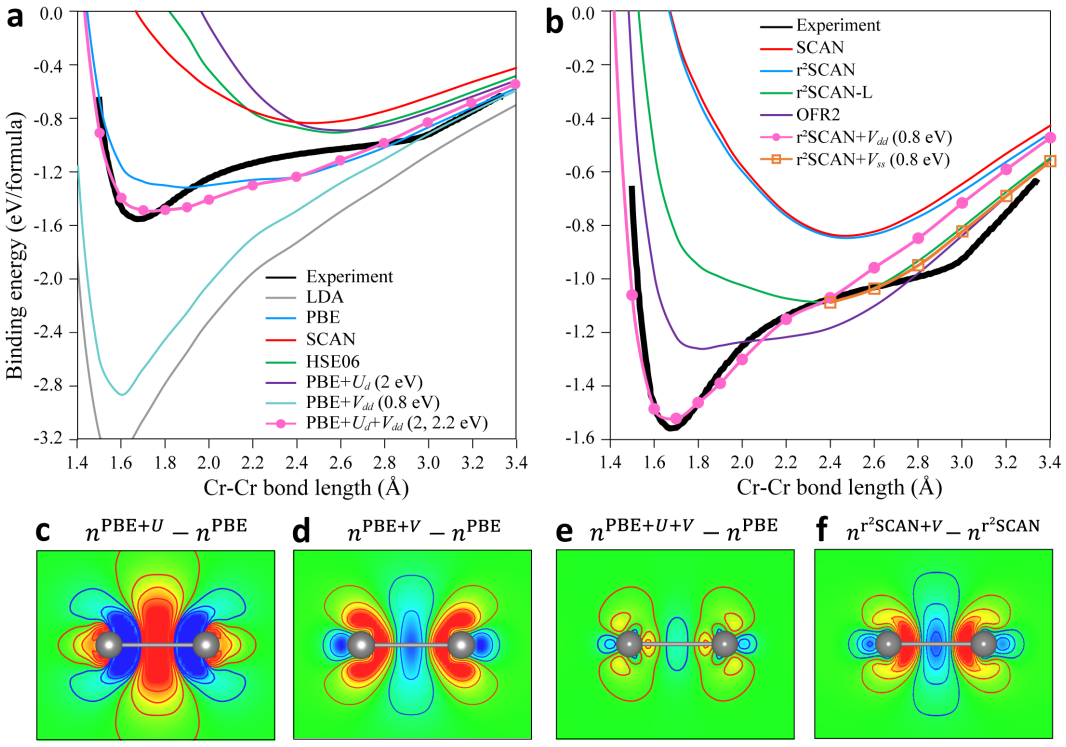

Figure 2.

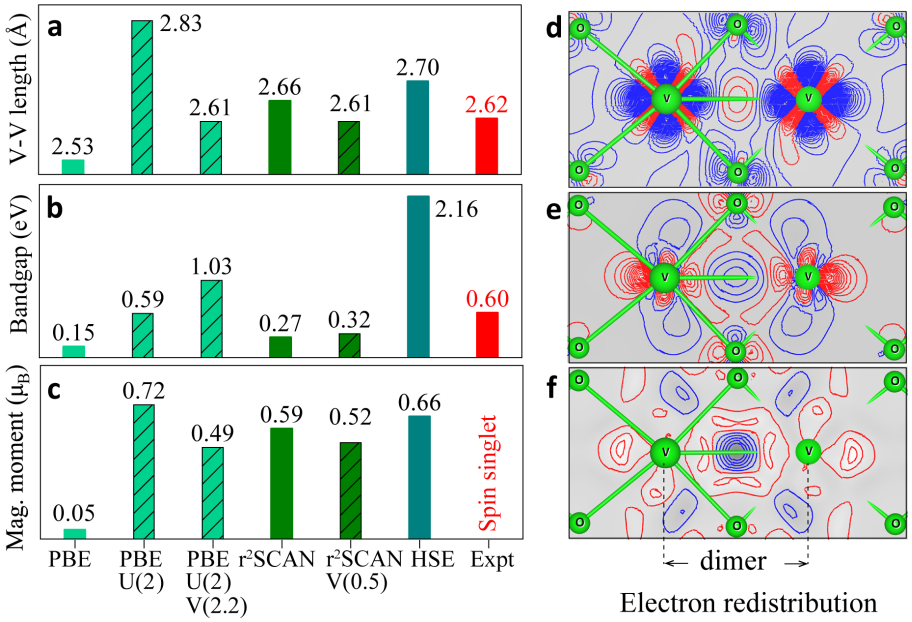

Figure 3.

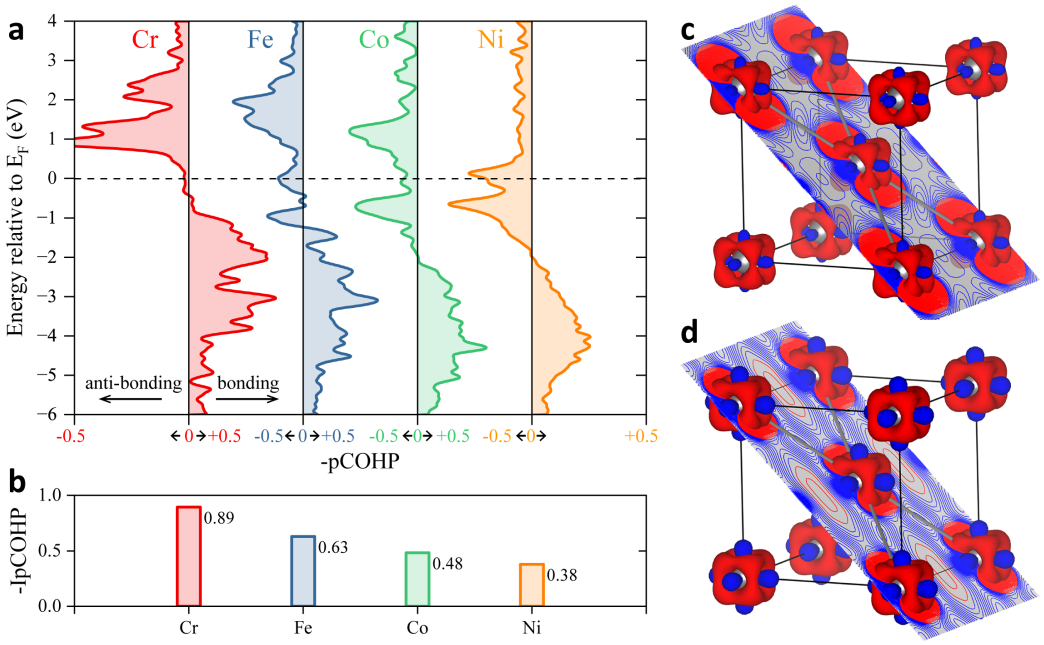

Figure 4.

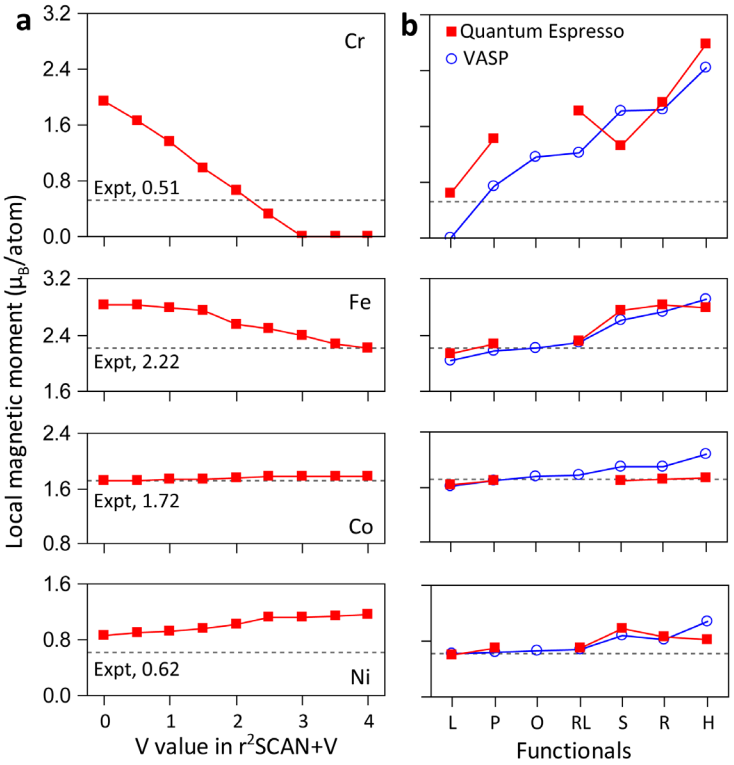

Figure 5.

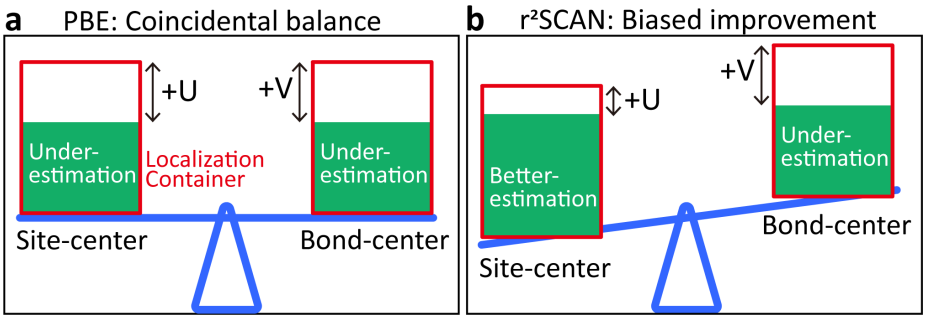

Figure 6.